Heterogeneous catalysts with programmable topologies generated by reticulation of organocatalysts into metal-organic frameworks: The case of squaramide

Anna Broto-Ribas[1,§], Claudia Vignatti[1,§], Alicia Jimenez-Almarza[2], Javier Luis-Barrera[3] , Zahra Dolatkhah[2] , Felipe Gándara[4] , Inhar Imaz[1 (*)], Rubén Mas-Ballesté[3,5 (*)], José Alemán[2,5 (*)], and Daniel Maspoch[1,6 (*)]

1 Catalan Institute of Nanoscience and Nanotechnology (ICN2), CSIC and The Barcelona Institute of Science and Technology, 08193 Barcelona, Spain
2 Inorganic Chemistry Department, Módulo 7, Universidad Autónoma de Madrid, 28049 Madrid, Spain
3 Organic Chemistry Department, Módulo 1, Universidad Autónoma de Madrid, 28049 Madrid, Spain
4 Materials Science Factory, Instituto de Ciencia de Materiales de Madrid (ICMM), Consejo Superior de Investigaciones Científicas (CSIC), Calle Sor Juana Inés de la Cruz, 3, 28049 Madrid, Spain
5 Institute for Advanced Research in Chemical Sciences (IAdChem), Campus Universidad Autónoma de Madrid, 28049 Madrid, Spain
6 Institució Catalana de Recerca i Estudis Avançats (ICREA), 08100 Barcelona, Spain
§ Anna Broto-Ribas and Claudia Vignatti contributed equally to this work.

ABSTRACT

A well-established strategy to synthesize heterogeneous, metal-organic framework (MOF) catalysts that exhibit nanoconfinement effects, and specific pores with highly-localized catalytic sites, is to use organic linkers containing organocatalytic centers. Here, we report that by combining this linker approach with reticular chemistry, and exploiting three-dimensioanl (3D) MOF-structural data from the Cambridge Structural Database, we have designed four heterogeneous MOF-based catalysts for standard organic transformations. These programmable MOFs are isoreticular versions of **pcu** IRMOF-16, **fcu** UiO-68 and pillared-**pcu** SNU-8X, the three most common topologies of MOFs built from the organic linker p,p'-terphenyldicarboxylic acid (tpdc). To synthesize the four squaramide-based MOFs, we designed and synthesized a linker, 4,4'-((3,4- dioxocyclobut- 1- ene- 1,2- diyl)bis(azanedyil))dibenzoic acid (Sq_tpdc), which is identical in directionality and length to tpdc but which contains organocatalytic squaramide centers. Squaramides were chosen because their immobilization into a framework enhances its reactivity and stability while avoiding any self-quenching phenomena. Therefore, the four MOFs share the same organocatalytic squaramide moiety, but confine it within distinct pore environments. We then evaluated these MOFs as heterogeneous H-bonding catalysts in organic transformations: a Friedel-Crafts alkylation and an epoxide ring-opening. Some of them exhibited good performance in both reactions but all showed distinct catalytic profiles that reflect their structural differences.

KEYWORDS reticular chemistry, metal-organic frameworks, H-bond catalysis, squaramide, Friedel-Crafts, epoxide ring-opening

Introduction

Metal-organic frameworks (MOFs) are crystalline porous compounds based on metal ions or clusters connected by organic ligands, whose topology, pore size and/or chemical composition can be modulated to achieve functionalities such as catalysis or adsorption. Those MOFs that exhibit confinement effects, and pores functionalized with specific and highly localized catalytic sites, are a potentially limitless source of new heterogeneous catalysts. Most reported MOF-based catalysts have been designed around metallic catalytic sites. In these, coordinatively unsaturated metal sites form the MOF structure itself, or metal ions/complexes/clusters/nanoparticles are encapsulated within the MOF pores or connected to the MOF organic linkers [1–5]. An alternative, less-explored approach to synthesizing heterogeneous MOF catalysts is to incorporate organocatalytic centers within MOFs [6, 7]. This can be done via postsynthetic modifications of the organic linkers in existing MOFs [8–12], or during MOF synthesis, by using organic linkers that contain these organocatalytic centers [13–28]. The latter approach in particular can benefit from reticular chemistry, which can facilitate rational design of MOF-based catalysts with pre-defined framework topologies and pores. Indeed, as Prof. O. M. Yaghi has affirmed, an important feature of reticular chemistry is that "for a given framework, the constituents can also be chemically functionalized either pre- or post-synthetically, while maintaining the framework's connectivity, to produce functionalized pores" [29, 30]. In our field, this idea translates to the ability to modify the organic linker of an existing MOF by inserting an organocatalytic center, without modifying the linker length or topology, thus enabling synthesis of the corresponding isoreticular MOF structure containing the desired center. Telfer *et al.* were among the first to prepare a MOF-based catalyst by this organocatalytic-center approach: an isoreticular MOF-5 with organocatalytic N-Boc-L-proline moieties that, after removing the thermolabile group, catalyzed aldol reactions [26]. Also, Kapteijn et al. reported the isoreticular NH2-MIL-101, showing high activity in base-catalyzed Knoevenagel condensations [22]. Soon afterwards, Farha, Hupp et al. similarly introduced H-bonding organocatalytic centers (e.g. urea and squaramide) into programmable MOFs [23–25]. For example, they synthesized two isoreticular UiO-67 catalysts from biphenyl-4,4'-dicarboxylate linkers functionalized with pendant urea and squaramide groups [23, 25]. This type of strategy has since been extended to many other isoreticular MOF-based catalysts containing urea moieties [19–21, 23, 24]. Herein we report the rational synthesis of four heterogeneous, MOF-based catalysts with programmable topologies, based on use of reticular chemistry and on MOF three-dimensional (3D)-structural information from the Cambridge Structural Database [31]. Briefly, we confined the same squaramide organocatalytic center into different MOFs that exhibit distinct nanoscale-pore environments. A

squaramide was chosen as the test case organocatalyst because it is known that its immobilization into a framework enhances its reactivity and stability while avoiding any self-quenching phenomena due to their tendency to self-aggregate in solution [6, 32]. The MOFs are isoreticular versions of **pcu** IRMOF-16, **fcu** UiO-68 and pillared-**pcu** SNU-8X, the three most common topologies of MOFs built from the organic linker p,p'-terphenyldicarboxylic acid (tpdc). Our four-step strategy (Fig. 1) entailed the design and synthesis of the linker, 4,4'-((3,4-dioxocyclobut-1-ene-1, 2-diyl)bis(azanedyil))dibenzoic acid (Sq_tpdc) [27], which is identical in directionality and length to tpdc but which contains organocatalytic squaramide centers. We evaluated the four MOF-based catalysts for H-bonding catalysis in a representative Friedel-Crafts alkylation and a representative epoxide ring-opening. Some of these MOFs exhibited good performance in both reactions but all showed distinct catalytic profiles that reflect their structural differences.

2 Experimental

2.1 Materials and methods

Zinc(II) nitrate hexahydrate ($Zn(NO_3)_2 \cdot 6H_2O$), zirconium(IV) oxychloride octahydrate ($ZrOCl_2 \cdot 8H_2O$), 4,4'-bipyridine and 2,5-bispyridylethane, dimethyl squarate, 4-aminobenzoic acid, trimethylamine, and anilines were purchased from commercial sources and used as received without further purification. 4,4'- ((3,4-Dioxocyclobut-1-ene-1,2-diyl)bis(azanediyl))dibenzene used as molecular catalyst (MC) was synthesized following a described procedure in Ref. [27]. Nuclear magnetic resonance (NMR) spectra were acquired on a Bruker Avance 300 MHz spectrometer, running at 300 MHz (1 H) or 75 MHz (13C). In some cases (noted), they were acquired on a Bruker Avance 250 MHz spectrometer. Chemical shifts (δ) were reported in ppm relative to residual solvent signals (CDCl3: 7.26 ppm for 1 H-NMR and 77.16 ppm for 13C-NMR; DMSO-d6: 2.50 ppm for 1 H-NMR and 39.52 ppm for 13C-NMR). Coupling constants were reported in Hertz. The following abbreviations are used to describe peak patterns: s (singlet), d (doublet), t (triplet), q (quartet), m (multiplet), bs (broad singlet). Different methods were used for measuring the exact mass (indicated for each case). Electrospray mass spectroscopy (MS (ESI)) spectra were acquired with an Agilent Technologies 6120 Quadrupole LC/MS. Electron ionization mass spectroscopy (MS (EI)) spectra were acquired with an Agilent Technologies 5977B MSD. For both techniques, MassWorks v. 4.0.0.0 (Cerno Bioscience) was used for the formula identification. MassWorks is MS-calibration software that calibrates for isotope profile as well as for mass accuracy, enabling highly accurate comparisons between calibrated and theoretical spectra. Electrospray mass spectroscopy with time-of-flight detector (MS (TOF-ESI)) spectra were acquired with microTOF-Q Bruker Daltonics spectrometer. Optical rotation was recorded in cells with 10-cm path-length; the solvents and concentrations (in g/100 mL) were

indicated in each case. Flash chromatography was performed on silica-gel columns (40 to 63 μm; pore size: 60 Å). Kinetics were studied by monitored reaction progress by gas chromatography using a 7820A GC System (Agilent Technologies) equipped with a flame ionization detector (FID). Elemental analyses were obtained on a EA1108 micro-analyzer (CarboErba). Volumetric N2 adsorption–desorption isotherms were collected at 77 K using an ASAP2020 HD (Micromeritics).

2.2 X-ray diffraction

Composition of all bulk materials was confirmed through X-ray powder diffraction (XRPD) measurements. They were collected on an X'Pert PRO MPD analytical diffractometer (Panalytical) at 45 kV and 40 mA using Cu Kα radiation (λ = 1.5419 Å) and compared with single-crystal simulated patterns. Single-crystal X-ray diffraction (SCXRD) data on Sq_IRMOF-16, Sq_UiO-68, Sq_SNU-8X and Sq_bptMOF were collected at 100(2) K in the BL13-XALOC beamline [33] at the ALBA synchrotron, on a single-axis goniometer with a Pilatus 6M detector using a monochromatic X-ray beam (λ = 0.82656 Å). Sq_SNU-8X and Sq_bptMOF were also collected at 293(2) K. The data frames were integrated and scaled using XDS software [34]. Absorption correction was not applied. All structures were solved by direct methods and subsequently refined by correction of F2 against all reflections, using SHELXT2013 and SHELXL2013 within the WinGX package and OLEX2 software [35, 36]. The framework atoms were located and refined. For both Sq_IRMOF-16 and Sq_UiO-68, the atoms belonging to the squaramide units were refined using rigid body constrains, and with partial occupancies, due to the disorder that they exhibit. Residual electron density was found inside the pores, likely corresponding to presence of disorder molecules. In all structures, attempts to adequately model the disordered molecules were unsatisfactory; therefore, the PLATON/SQUEEZE routine was applied to mask out the disordered electron density [37].

2.3 Synthesis of 4-((2-methoxy-3,4-dioxocyclobut-1- en-1-yl)amino)benzoic acid

A white suspension of dimethyl squarate (1.00 g, 7.00 mmol) and 4-aminobenzoic acid (0.960 g, 7.00 mmol) in 20 mL of dry MeOH was stirred 24 h at room temperature. The resulting yellow suspension was filtered, washed with MeOH and Et_2O, and then dried under vacuum to afford the desired pure compound 4-((2-methoxy-3,4-dioxocyclobut-1-en-1-yl)amino)benzoic acid (1.30 g, 5.26 mmol, 75% yield). 1 H-NMR (300 MHz, DMSO-d6): δ 12.71 (bs, 1H), 10.96 (s, 1H), 7.94–7.86 (m, 2H), 7.50–7.40 (m, 2H), 4.40 (s, 3H). 13C-NMR (75 MHz, DMSO-d6): δ 187.6, 184.4, 179.5, 169.1, 166.8, 142.0, 130.6, 125.7, 118.7, 60.7.

2.4 Synthesis of 4,4'-((3,4-dioxocyclobut-1-ene-1,2- diyl)bis(azanediyl))dibenzoic acid (Sq_tpdc)

A mixture of 4-((2-methoxy-3,4-dioxocyclobut-1-en-1-yl) amino)benzoic acid (0.90 g, 3.60 mmol), 4-aminobenzoic acid (0.497 g, 3.60 mmol) and Et_3N (0.503 mL, 3.60 mmol) in 18 mL of dry CH_3CN in a sealed tube was heated at 80 °C for 24 h. The resulting suspension was concentrated down to ca. 9 mL. Then, H_2O (20 mL) was added, and the pH was adjusted to 1 (conc. HCl). The solid was filtered and washed thoroughly with H2O until neutral pH, washed with Et2O and finally, dried under vacuum to afford pure squaramide Sq_tpdc (1.01 g, 2.87 mmol, 80% yield). 1 H-NMR (250 MHz, DMSO-d6): δ 12.72 (bs, 2H), 10.31 (bs, 2H), 7.94 (d, J = 8.4 Hz, 4H), 7.57 (d, J = 8.4 Hz, 4H). 13C-NMR (63 MHz, DMSO-d6): δ 182.0, 166.8, 165.9, 142.4, 130.9, 125.1, 118.0. MS (TOF-ESI-): calculated for C18H11N2O6 − ([M−H]−): 351.0623. Found: 351.0614.

2.5 Synthesis of Sq_IRMOF-16

$Zn(NO_3)_2 \cdot 6H_2O$ (0.017 g, 0.057 mmol) and Sq_tpdc (0.020 g, 0.057 mmol) were dissolved in 4.8 mL DMF and heated to 85 °C for 7 days. This afforded yellow cubic crystals (0.010 g; 0.0075 mmol, 53% yield), which were stored in DMF. FT-IR (ATR; cm−1): 1,650 (C=O from carboxylate) selected band. Anal. calcd. for ($[Zn_4O(L1)_3] \cdot 6H_2O \cdot 4DMF$; $Zn_4C_{66}H_{70}N_{10}O_{29}$): C, 45.85; H, 4.08; N, 8.10, found: C, 45.23; H, 3,97; N, 8.34

2.6 Synthesis of the Sq_UiO-68

A DMF solution (4 mL) of Sq_tpdc (20 mg, 0.057 mmol) and $ZrOCl_2 \cdot 8H_2O$ (18.31 mg, 0.057 mmol) were added 5 mL of a DMF/formic acid mixture (4:1 w/w). The mixture was heated at 120 °C for 1 week. This afforded yellow crystals, which were filtered, washed with DMF and MeOH, and then, air-dried to give Sq_UiO-68 (22.3 mg; 0.008 mmol, 84%). FT-IR (ATR; cm−1, selected bands): 3,167 (OH); 2,927 (NH); 1,793, 1,647 (C=O from DMF); 1,597 (C=O from carboxylate). Anal. calcd. for ([Zr6O4(OH)4(L1)6]; Zr6C108H64N12O44): C, 46.64; H, 2.32; N, 6.04, found: C, 47.12; H, 2,58; N, 7,00.

2.7 Synthesis of Sq_SNU-8X

$Zn(NO_3)_2 \cdot 6H_2O$ (0.017 g, 0.057 mmol), Sq_tpdc (0.020 g, 0.057 mmol) and 4,4'-bipyridine (0.009 g, 0.057 mmol) were dissolved in 4.8 mL DMF. The mixture was placed in a 10-mL Erlenmeyer flask, which was covered with a septum, and then heated to 85 °C for 5 days. This afforded yellow crystals (0.016 g; 0.015 mmol, 53% yield). FT-IR (ATR; cm−1, selected bands): 3,200 (OH), 1,788, 1,639, 1,598 (C=O from carboxylate), 1,558, 1,488, 1,367, 1,240, 1,180, 1,100, 777, 636, 475. Anal. calcd. for Zn2C55H49N9O15: C, 54.74; H, 4.09; N, 10.45, found: C, 54.30; H, 3.94; N, 10.60.

2.8 Synthesis of Sq_BptMOF

$Zn(NO_3)_2 \cdot 6H_2O$ (0.017 g, 0.057 mmol), Sq_tpdc (0.020 g, 0.057 mmol) and 1,2-bis(4-pyridyl)ethane (0.010 g, 0.057 mmol) were dissolved in 4.8 mL DMF. The mixture was placed in a 10-mL Erlenmeyer flask, which was covered with a septum, and then heated to 85 °C for 5 days. This afforded orange crystals (0.013 g; 0.013 mmol, 45% yield). FT-IR (ATR; cm−1, selected bands): 3,200 (OH), 1,787, 1,703, 1,644 (C=O from carboxylate), 1,602, 1,543, 1,493, 1,440, 1,241, 1,177, 1,102, 775. Anal. calcd. for Zn2C54H54N8O18: C, 52.57; H, 4.41; N, 9.08, found: C, 52.00; H, 4.16; N, 9.20.

2.9 Catalysis experiments

A 0.005 mmol-(squaramide equivalent) aliquot of a single, dried MOF-based catalyst (2.8 mg of Sq_IRMOF-16; 2.9 mg of Sq_SNU-8X; 2.9 mg of Sq_BptMOF; or 2.4 mg of Sq_UiO-68), 0.1 mmol (12.3 mg) of p-methoxyaniline and a stirring bar were transferred to a septum-sealed vial, which was flushed with N2 for 15 min. Note that Sq_SNU-8X, Sq_BptMOF, and Sq_UiO-68 were incubated in methanol for 72 h before use. Then, 200 μL of ethyl epoxide was added to the mixture. The mixture was heated to 60 °C and stirred for 8 h. At different time-points (1, 2, 4, 6 and 8 h), a 20-μL aliquot of the reaction mixture was removed, and then diluted with 500 μL of a 0.005 M solution of 2-methylnaphthalene (gas chromatography standard) in toluene. The resulting sample was then analyzed by gas chromatography with FID. For the Friedel-Craft reaction, a 0.01 mmol-aliquot of a single, dried MOF-based catalyst (5.6 mg of Sq_IRMOF-16; 4.9 mg of Sq-UiO-68; 5.7 mg of Sq_SNU-8X; or 5.8 mg of Sq_bptMOF), 0.15 mmol of indole, 0.10 mmol of β-nitrostyrene and a stirring bar were transferred to a septum-sealed vial. Then, 1 mL of toluene was added to the mixture. The mixture was heated to 60 °C and stirred for 3 days. At different timepoints (4, 7, 24, 48 and 72 h), a 100-μL aliquot of the reaction mixture was removed, and then diluted with 500 μL of a 0.005 M solution of 2-methylnaphthalene (gas chromatography standard) in toluene. The resulting sample was then analyzed by gas chromatography with FID.

3 Results and discussion.

3.1 Design, synthesis and analysis of the squaramide based linker

We designed the linker Sq_tpdc by attaching two benzoic acid moieties to the NH groups of the squaramide (Fig. 1), which was justified based on two factors. Firstly, we reasoned that the phenyl rings would favor structural planarity and rigidity in the linker, while the two opposing carboxyl groups would enable construction of extended structures via metal ion coordination. Secondly, we sought to exploit the para position of squaramide groups relative to the carboxyl groups, to maximize the acidity of the squaramide-NH protons. Specifically, the electron-withdrawing nature of the carboxylic groups acts by resonance in the ortho and para positions, thereby diminishing the electron density of the NH groups and increasing their acidity and, consequently,

their ability to form hydrogen bonds (i.e. to catalyze H-bonding reactions). We further reasoned that since the squaramide ring is roughly equivalent in size to a phenyl ring, then the carboxylic groups of Sq_tpdc would be separated by a distance very close (14.6 Å) to that corresponding to three phenyl rings (14.4 Å). Accordingly, we considered that Sq_tpdc is roughly equivalent in both directionality (topology) and length to tpdc (Fig. 1), a wellknown dicarboxylate linker in MOF synthesis [38–40]. Once we had designed Sq_tpdc, we synthesized it by a previously-reported, two-step method [27].

3.2 Cambridge Structural Database search

We searched the Cambridge Crystallographic Data Centre (CCDC) database (ConQuest v. 2.0.0, CCDC, Cambridge, UK) for 3D MOF structures built from tpdc. We found three structures, which we classified into two framework topologies: two of the structures corresponded to IRMOF-16 MOF (**pcu** topology; one non-interpenetrated framework and one double-interpenetrated framework (this latter also known as IRMOF-15); Fig. 2(a)); and the third one, to UiO-68 MOF (**fcu** topology; Fig. 2(b)). The **pcu** IRMOF-16 comprises Zn4O clusters linked to six tpdc linkers in an octahedral coordination. The non-interpenetrated IRMOF-16 contains cubic cavities delimited by twelve tpdc linkers, with a pore opening of ca. 15 Å [40]. The **fcu** UiO-68 comprises octahedral $[Zr_6O_4(OH)_4]$ clusters linked by twelve tpdc linkers that create two types of spaces between them: octahedral cavities delimited by twelve tpdc linkers, and tetrahedral cavities delimited by six tpdc linkers, both showing trigonal pore openings of ca. 10 Å [38, 39]. To extend the number of potential 3D MOF structures that could be synthesized using Sq_tpdc, we also searched for 3D MOF structures built from tpdc functionalized at any of the four aromatic positions of the central phenyl ring by groups that cannot coordinate to metal ions (i.e. to maintain the directionality of the parent tpdc). This revealed 53 additional 3D structures: fifteen (28%) of which exhibit **fcu** topology and six (11%) of which, **pcu** topology [41–54]. Of the remaining 32 structures, eighteen (24%) correspond to pillared-**pcu** MOFs (Figs. 2(c) and 2(d)) [55–59]. In these latter MOFs, paddle-wheel M2 (M = Zn(II), Cu(II) and Cd(II)) clusters are bridged by four tpdc linkers that form 2D square grids, which are linked by pillared N-based linkers that form 3D structures with bidirectional one-dimensional (1D) pores. These pores are delimited by four tpdc linkers and by two tpdc and two pillared linkers. In some cases, the pillared linkers are not truly perpendicular to the cluster-carboxylic layers and the pores are distorted prisms with rhombic windows. The fourteen remaining structures pertain to four MOF topology groups: eight (15%) of them comprise planes or chains of metal oxides (M = Co(II), Ni(II), Mn(II), Pb(II), Mg(II), Eu(III) and Cd(II)) linked by tpdc linkers; three (6%) of them exhibit a diamond topology [60, 61]; two (4%) of them, **acs** topology [62, 63]; and one (2%) of them, **bcu** topology [41]. The diamond MOFs are formed by linkage of tetrahedral Zn(II) or Cd(II) ions through two tpdc and two N,N'-based linkers. The **acs** MOFs are formed through linkage of trigonal M_3O (M = Fe(III)

and In(III)) clusters by six tpdc linkers (two linkers per edge). Both structures show pores with the shape of a bipyramidal trigonal base (or a slightly distorted tetrahedron) delimited by six tpdc ligands with (slightly distorted) hexagonal windows of ca. 19 Å. The **bcu** MOF is formed by octahedral $[Zr_6O_8(OH_2)_8]$ clusters coordinated by eight tpdc linkers that generate octahedral pores, which are delimited by eight tpdc linkers and exhibit rhombic windows of ca. 13 Å.

3.3 Selection, synthesis and structural analysis of isoreticular MOFs

After the Cambridge Structural Database search, we selected the three most common MOF topologies and investigated the synthesis of the corresponding isoreticular MOFs incorporating the squaramide moieties. Here, we chose both **pcu** IRMOF-16 and **fcu** UiO-68 frameworks (Figs. 2(a) and 2(b)), as they are the only two topologies reported using the non-functionalized tpdc linker and are highly abundant, together corresponding to 41% of all reported 3D structures. We also chose pillared-**pcu** MOFs (Figs. 2(c) and 2(d)), due to their rich potential for obtaining myriad compositions by simply exchanging the pillared linker, and because they, too, are highly abundant (32% of all reported 3D structures). Here, we used bipy and bpt linkers as the pillars, aiming to synthesize isoreticular versions of SNU-8X (hereafter, Sq_SNU-8X) and OZASUF (hereafter, Sq_bptMOF) [57]. Characterization of the synthesized Sq_IRMOF-16 crystals by SCXRD confirmed that they retain the characteristic IRMOF-16 **pcu** topology (Fig. 2(a) and Table S1 in the Electronic Supplemenary Material (ESM)). Thus, Sq_IRMOF-16 exhibits a 3D structure built from the connection of Zn4O clusters through six Sq_tpdc linkers to form the expected cubic cavities delimited by twelve Sq_tpdc linkers and showing a pore opening of 14 Å (Fig. 1(a); Brunauer–Emmett–Teller surface area SBET measured by N2 sorption at 77 K of 784 m2 /g; Fig. S6 in the ESM). However, in this structure, the squaramide rings of the Sq_tdpc linkers exhibit high mobility and positional disorder: They could only be partly positioned during the SCXRD refinement, even when it was performed at 100 K. Accordingly, their position and orientation were refined by employing rigid-body restraints, which revealed that Sq_ IRMOF-16 has cubic cavities containing zero, four or eight squaramide rings pointing towards them (Fig. 2(a)). However, given the high mobility of the squaramide rings, each cubic cavity could also be statistically considered to contain three rings pointing towards it. Characterization of the synthesized Sq_UiO-68 crystals by SCXRD confirmed formation of the desired analogous fcu UiO-68 structure (Fig. 2(b) and Table S2 in the ESM) [14]. According to the SCXRD refinement, the Sq_tpdc linker exhibits positional disorder, as evidenced by the splitting in the position of some of the carbon atoms in the phenyl rings. This implies different possible orientations of the squaramide units. Thus, the atoms in the squaramide moieties of the Sq_tpdc linkers were refined with the use of rigid body constrains and partial occupancies after being located in the density maps. Overall, Sq_UiO-68 exhibits a fcu topology in which $[Zr_6O_4(OH)_4]$ nodes are connected via 12 Sq_tpdc ligands forming a porous network (S_{BET} = 637 m2 /g; Fig. S8 in the ESM). This

network shows octahedral cavities and tetrahedral cavities delimited by twelve and six Sq_tpdc linkers, respectively, and connected by windows of 7 Å. In these cavities, six squaramide rings are pointing towards the octahedron cavities (Fig. 2(b)). Similarly to the previous examples, SCXRD of the synthesized Sq_SNU-8X crystals revealed formation of the expected pillared MOF with **pcu** topology (Fig. 2(c) and Table S3 in the ESM). The basic Sq_SNU-8X units are paddle-wheel Zn_2 clusters, in which each Zn(II) ion exhibits square-pyramidal coordination geometry. The equatorial sites of the pyramid are occupied by four oxygen atoms of the carboxylate groups of four Sq_tpdc linkers, whereas the last axial coordination position is occupied by a nitrogen atom of the N-donor bipy linker. The resulting paddle-wheel Zn2 clusters are connected through four Sq_tpdc linkers that form two-dimensional (2D) square grids, which in turn are connected by bipy linkers that form 3D **pcu** nets, which are doubly interpenetrated. Note that the parent SNU-8X is also a doubly-interpenetrated MOF. Interpenetrated Sq_SNU-8X possesses 1D channels of two sizes: 12 Å × 12 Å, delimited by four Sq_tpdc and running along the a-axis; and 8 Å × 12 Å, delimited by two Sq_tpdc and two bipy linkers and running along the c-axis (Fig. 2(c)). The squaramide rings are parallel to the pores along the a-axis but point towards those along the c-axis. Based on these apparent voids and free channels, the porosity of Sq_SNU-8X was evaluated by measuring its N_2 sorption at 77 K, which gave an S_{BET} value of 634 m^2/g (Fig. S10 in the ESM). We also prepared Sq_bptMOF by using the same conditions as for Sq_SNU-8X, except that instead of bipy, we used bpt. Interestingly, SCXRD revealed formation of a doubleinterpenetrated pillared **pcu** MOF (SBET = 789 m^2/g, Table S4 and Fig. S13 in the ESM) much like that in Sq_SNU-8X, as it similarly contained 1D channels of two sizes: 8 Å × 11 Å, delimited by two Sq_tpdc and two bipy linkers and running along the a-axis; and 12 Å × 11 Å, delimited by four Sq_tpdc linkers and running along the c-axis (Fig. 2(d)). In this case, the squaramide rings point towards the pores along the a-axis but are parallel to those along the c-axis. Finally, as these type of pillared **pcu** MOFs (including the isoreticular SNU-8X and OZASUF) [57] tend to show structural flexibility upon solvent removal, we also solved the crystal structures of both Sq_SNU-8X and Sq_bptMOF at 293 K (Tables S5 and S6 and Figs. S11 and S14 in the ESM). As expected, both frameworks showed to be flexible, with Sq_ bptMOF exhibiting a decrease of its pore sizes (6.5 Å × 11 Å and 11.5 Å × 11 Å) at 293 K. 3.4 Evaluation of catalytic performance We hypothesized that synthesis of diverse heterogeneous catalysts using our reticular approach, followed by catalytic screening of them in test reactions, would greatly augment the probability of finding high-performing catalysts for any desired chemistry. Thus, we evaluated our MOF-based catalysts in two archetypical, squaramide-catalyzed reactions: a representative Friedel-Crafts alkylation and a representative epoxide ring-opening. Importantly, XRPD performed during and after these two catalytic reactions confirmed the crystallinity and stability of squaramide-based MOFs (Figs. S15–S18 in the ESM); albeit Sq_bptMOF showed a certain loss of crystallinity after both catalytic reactions. The stability of squaramide-based MOF

was further corroborated by discarding the leaching of catalytic species into the reaction media. Such feature was assessed by means of experiments consisting on filtering off the catalytic material at intermediate stages of each reaction, observing that product content did not evolve further after MOF removal. Crucially, when the molecular squaramide 4,4'- ((3,4-dioxocyclobut-1-ene-1,2-diyl)bis(azanediyl))dibenzene was used alone as catalyst, both reactions barely progressed, likely due to its self-aggregation and poor solubility. This result supported our original strategy of designing heterogeneous catalysts in which the squaramide rings are immobilized within MOFs. We then studied the kinetics of a representative Friedel-Crafts alkylation: reaction of indole (0.15 mmol) and β-nitrostyrene (0.10 mmol) in the presence of the corresponding squaramidebased MOFs (0.005 mmol = 5 mol% (catalytic centers) relative to β-nitrostyrene) at 60 °C. Figure 3 is a plot of the kinetics for each squaramide-based MOF catalyst over 72 h. The most active catalyst for this reaction was Sq_SNU-8X (yield: 85%) followed by Sq_UiO-68 and Sq-IRMOF-16 (yield for each: ca. 70%), and finally, Sq_bptMOF (yield: 18%). We attributed the low performance of Sq_bptMOF to the structural flexibility already observed by SCRXD at 293 K and XRPD (Fig. S18 in the ESM). Note that structural flexibility is commonly observed when flexible pillar ligands such as bpt, which have a high degree of rotation freedom due to the $–CH_2–CH_2–$ chain between the pyridine fragments, are used to synthesize pillared **pcu** MOFs [57]. This highly dynamic behavior impedes catalytic Figure 3 Kinetic plots for the Friedel-Crafts reaction of indole and β-nitrostyrene at 60 °C, forming the alkylated product, in the presence of Sq_IRMOF-16 (yellow), Sq_SNU-8X (orange), Sq_UiO-68 (blue) or Sq_bptMOF (grey performance, as it decreases the pore size and therefore accessibility of the substrates to the active sites. We next studied the kinetics of a representative epoxide ring-opening: reaction of 4-methoxy aniline (0.1 mmol) and ethyl epoxide (molar excess) at 60 °C in the presence of the corresponding squaramide-based MOF (0.005 mmol = 5 mol% (catalytic centers) relative to 4-methoxy aniline) for 8 h. Figure 4 shows the kinetics of the ring-opening reaction. This reaction can consecutively generate two products: the mono-addition and bis-addition products. The best catalysts for the formation of the bis-addition product were Sq_IRMOF-16 and Sq_ SNU-8X, which gave nearly quantitative transformation after 8 h. In contrast, Sq_UiO-68 and Sq_bptMOF gave roughly 50/50 mixtures of the mono-addition and bis-addition products after 8 h. Figure 4 Kinetic plots for the epoxide ring-opening reaction of 4-methoxy aniline (blue) and ethyl epoxide at 60 °C to form the mono-adduct (orange) or bis-adduct (grey) product, in the presence of Sq_IRMOF-16, Sq_SNU-8X, Sq_UiO-68 or Sq_bptMOF. We explained this discrepancy in catalytic performance according to sterics. Specifically, formation of the bis-adduct from the double epoxide ring-opening process appears to be highly sterically demanding and sensitive to aperture sizes. Accordingly, the most sterically-restricted MOFs would be the worse catalysts for the double-epoxide activation. This was indeed the case for the flexible Sq_bptMOF (vide supra) as well as for Sq_UiO-68, which has a smaller pore opening (7 Å) than Sq_IRMOF-16 (14 Å)

and Sq_SNU-8X (12 Å). 4 Conclusions In summary, we have reported the design, synthesis and testing of heterogeneous, MOF-based catalysts containing squaramide organocatalysts trapped within their pores. We demonstrated that organocatalytic MOFs with programmable topologies can be synthesized by exploiting reticular chemistry and 3D MOF-structural data from the Cambridge Structural Database. Our approach entailed design and synthesis of a new dicarboxylate linker containing the squaramide ring, Sq_tpdc, which was used to prepare four MOF-based catalysts that share the same organocatalytic center but differ in their pore environments. The MOFs are isoreticular versions of **pcu** IRMOF-16, **fcu** UiO-68 and pillared-**pcu** SNU-8X, the three most common topologies of MOFs built from the organic linker tpdc, which is similar in length and directionality to Sq_tpdc. Sq_SNU-8X was the best catalyst in a representative Friedel-Crafts alkylation, whereas Sq_IRMOF-16 and Sq_SNU8X were the best in a representative epoxide ring-opening (formation of the bis-addition product). Using an approach like ours, researchers could ultimately design an entire catalog of MOF-based catalysts, thereby greatly increasing the chances of finding high-performance catalysts for targeted chemistries.

Acknowledgements

This work was supported by the Spanish MINECO (projects RTI2018-095622-B-I00 and RTI2018-095038-B-I00), the Catalan AGAUR (project 2017 SGR 238), the ERC under the EU FP7 (ERC−Co 615954), European Union's Horizon 2020 research and innovation program under grant agreement No. 685727, and European Structural Funds (S2018/NMT-4367). It was also funded by the CERCA Program/Generalitat de Catalunya. ICN2 is supported by the Severo Ochoa program from the Spanish MINECO (Grant No. SEV-2017-0706).

Electronic Supplementary Material: Supplementary Material (NMR, N2 isotherms, FT-IR, crystallographic tables, and XRPD) is available in the online version of this article at https://doi.org/10.1007/s12274-020-2779-8.

References

[1] Huang, Y. B.; Liang, J.; Wang, X. S.; Cao, R. Multifunctional metalorganic framework catalysts: Synergistic catalysis and tandem reactions. *Chem. Soc. Rev.* **2017**, *46*, 126–157.

[2] Dhakshinamoorthy, A.; Li, Z. H.; Garcia, H. Catalysis and photocatalysis by metal organic frameworks. *Chem. Soc. Rev.* **2018**, *47*, 8134–8172.

[3] Liu, J. W.; Chen, L. F.; Cui, H.; Zhang, J. Y.; Zhang, L.; Y. Su, C. Y. Applications of metal-organic frameworks in heterogeneous supramolecular catalysis. *Chem. Soc. Rev.* **2014**, *43*, 6011–6061.

[4] Huang, Y. B.; Lin, Z. J.; Cao, R. Palladium nanoparticles encapsulated in a metal-organic framework as efficient heterogeneous catalysts for direct C2 arylation of indoles. *Chem.—Eur. J.* **2011**, *17*, 12706– 12712.

[5] Huang, Y. B.; Wang, Q.; Liang, J.; Wang, X. S.; Cao, R. Soluble metal-nanoparticle-decorated porous coordination polymers for the homogenization of heterogeneous catalysis. *J. Am. Chem. Soc.* **2016**, *138*, 10104–10107.

[6] Alegre-Requena, J. V.; Marqués-López, E.; Herrera, R. P.; Díaz, D. D. Metal-organic frameworks (MOFs) bring new life to hydrogenbonding organocatalysts in confined spaces. *CrystEngComm* **2016**, *18*, 3985–3995.

[7] Rao, P. C.; Mandal, S. Potential utilization of metal-organic frameworks in heterogeneous catalysis: A case study of hydrogen-bond donating and single-site catalysis. *Chem.—Asian J.* **2019**, *14*, 4087–4102.

[8] Dong, X. W.; Liu, T.; Hu, Y. Z.; Liu, X. Y.; Che, C. M. Urea postmodified in a metal-organic framework as a catalytically active hydrogenbond-donating heterogeneous catalyst. *Chem. Commun.* **2013**, *49*, 7681–7683.

[9] Luan, Y.; Zheng, N. N.; Qi, Y.; Tang, J.; Wang, G. Merging metalorganic framework catalysis with organocatalysis: A thiourea functionalized heterogeneous catalyst at the nanoscale. *Catal. Sci. Technol.* **2014**, *4*, 925–929.

[10] Garibay, S. J.; Wang, Z. Q.; Cohen, S. M. Evaluation of heterogeneous metal-organic framework organocatalysts prepared by postsynthetic modification. *Inorg. Chem.* **2010**, *49*, 8086–8091.

[11] Zang, Y. D.; Shi, J.; Zhang, F. M.; Zhong, Y. J.; Zhu, W. D. Sulfonic acidfunctionalized MIL-101 as a highly recyclable catalyst for esterification. *Catal. Sci. Technol.* **2013**, *3*, 2044–2049.

[12] Aguado, S.; Canivet, J.; Schuurman, Y.; Farrusseng, D. Tuning the activity by controlling the wettability of MOF eggshell catalysts: A quantitative structure-activity study. *J. Catal.* **2011**, *284*, 207–214.

[13] Zhang, X. P.; Zhang, Z. J.; Boissonnault, J.; Cohen, S. M. Design and synthesis of squaramide-based MOFs as efficient MOF-supported hydrogen-bonding organocatalysts. *Chem. Commun.* **2016**, *52*, 8585– 8588.

[14] Cohen, S. M.; Zhang, Z. J.; Boissonnault, J. A. Toward "metalloMOFzymes": Metal-organic frameworks with single-site metal catalysts for small-molecule transformations. *Inorg. Chem.* **2016**, *55*, 7281–7290.

[15] Tehrani, A. A.; Abedi, S.; Morsali, A.; Wang, J.; Junk, P. C. Ureacontaining metal-organic frameworks as heterogeneous organocatalysts. *J. Mater. Chem. A* **2015**, *3*, 20408–20415.

[16] Rao, P. C.; Mandal, S. Friedel–Crafts alkylation of indoles with nitroalkenes through hydrogen-bond-donating metal–organic framework. *ChemCatChem* **2017**, *9*, 1172–1176.

[17] Hall, E. A.; Redfern, L. R.; Wang, M. H.; Scheidt, K. A. Lewis acid activation of a hydrogen bond donor metal-organic framework for catalysis. *ACS Catal.* **2016**, *6*, 3248–3252.

[18] Markad, D.; Mandal, S. K. Design of a primary-amide-functionalized highly efficient and recyclable hydrogen-bond-donating heterogeneous catalyst for the Friedel-Crafts alkylation of indoles with β-nitrostyrenes. *ACS Catal.* **2019**, *9*, 3165–3173.

[19] Ju, Z. F.; Yan, S. C.; Yuan, D. Q. De novo tailoring pore morphologies and sizes for different substrates in a urea-containing MOFs catalytic platform. *Chem. Mater.* **2016**, *28*, 2000–2010.

[20] Zhang, H.; Gao, X. W.; Wang, L.; Zhao, X. S.; Li, Q. Y.; Wang, X. J. Microwave-assisted synthesis of urea-containing zirconium metalorganic frameworks for heterogeneous catalysis of Henry reactions. *CrystEngComm* **2019**, *21*, 1358–1362.

[21] Wang, X. J.; Li, J.; Li, Q. Y.; Li, P. Z.; Lu, H.; Lao, Q. Y.; Ni, R.; Shi, Y. H.; Zhao, Y. L. A urea decorated (3,24)-connected rht-type metalorganic framework exhibiting high gas uptake capability and catalytic activity. *CrystEngComm* **2015**, *17*, 4632–4636.

[22] Serra-Crespo, P.; Ramos-Fernandez, E. V.; Gascon, J.; Kapteijn, F. Synthesis and characterization of an amino functionalized MIL-101(Al): Separation and catalytic properties. *Chem. Mater.* **2011**, *23*, 2565–2572.

[23] Siu, P. W.; Brown, Z. J.; Farha, O. K.; Hupp, J. T.; Scheidt, K. A. A mixed dicarboxylate strut approach to enhancing catalytic activity of a de novo urea derivative of metal–organic framework UiO-67. *Chem. Commun.* **2013**, *49*, 10920–10922.

[24] Roberts, J. M.; Fini, B. M.; Sarjeant, A. A.; Farha, O. K.; Hupp, J. T.; Scheidt, K. A. Urea metal–organic frameworks as effective and sizeselective hydrogen-bond catalysts. *J. Am. Chem. Soc.* **2012**, *134*, 3334– 3337.

[25] McGuirk, C. M.; Katz, M. J.; Stern, C. L.; Sarjeant, A. A.; Hupp, J. T.; Farha, O. K.; Mirkin, C. A. Turning on catalysis: Incorporation of a hydrogen-bond-donating squaramide moiety into a Zr metalorganic framework. *J. Am. Chem. Soc.* **2015**, *137*, 919–925.

[26] Lun, D. J.; Waterhouse, G. I. N.; Telfer, S. G. A general thermolabile protecting group strategy for organocatalytic metal-organic frameworks. *J. Am. Chem. Soc.* **2011**, *133*, 5806–5809.

[27] Vignatti, C.; Luis-Barrera, J.; Guillerm, V.; Imaz, I.; Mas-Ballesté, R.; Alemán, J.; Maspoch, D. Squaramide-IRMOF-16 analogue for catalysis of solvent-free, epoxide ring-opening tandem and multicomponent reactions. *ChemCatChem* **2018**, *10*, 3995–3998.

[28] Liang, J.; Chen, R. P.; Wang, X. Y.; Liu, T. T.; Wang, X. S.; Huang, Y. B.; Cao, R. Postsynthetic ionization of an imidazole-containing metalorganic framework for the cycloaddition of carbon dioxide and epoxides. *Chem. Sci.* **2017**, *8*, 1570–1575.

[29] Yaghi, O. M. Reticular chemistry in all dimensions. *ACS Cent. Sci.* **2019**, *5*, 1295–1300.

[30] Yaghi, O. M. Reticular chemistry: Molecular precision in infinite 2D and 3D. *Mol. Front. J.* **2019**, *3*, 66–83.

[31] Groom, C. R.; Bruno, I. J; Lightfoot, M. P.; Ward, S. C. The Cambridge structural database. *Acta Crystallogr. B Struct. Sci. Cryst. Eng. Mater.* **2016**, *B72*, 171–179.

[32] Storer, R. I.; Aciro, C.; Jones, L. H. Squaramides: Physical properties, synthesis and applications. *Chem. Soc. Rev.* **2011**, *40*, 2330–2346.

[33] Juanhuix, J.; Gil-Ortiz, F.; Cuni, G.; Colldelram, C.; Nicolás, J.; Lidón, J.; Boter, E.; Ruget, C.; Ferrer, S.; Benach, J. Developments in optics and performance at BL13-XALOC, the macromolecular crystallography beamline at the Alba Synchrotron. *J. Synchrotron Radiat.* **2014**, *21*, 679–689.

[34] Kabsch, W. XDS. *Acta Crystallogr. Sect. D* **2010**, *66*, 125–132.

[35] Sheldrick, G. SHELXT—Integrated space-group and crystal-structure determination. *Acta Crystallogr. Sect. A.* **2015**, *71*, 3–8.

[36] Dolomanov, O. V.; Bourhis, L. J.; Gildea, R. J.; Howard, J. A. K.; Puschmann, H. OLEX2: A complete structure solution, refinement and analysis program. *J. Appl. Cryst.* 2009, **42**, 339–341.

[37] Spek, A. L. PLATON/SQUEEZE. Acta Cryst. **2020**, *E76*, 1–11

[38] Manna, K.; Ji, P. F; Lin, Z. K.; Greene, F. X.; Urban, A.; Thacker, N. C.; Lin, W. B. Chemoselective single-site Earth-abundant metal catalysts at metal-organic framework nodes. *Nat. Commun.* **2016**, *7*, 12610.

[39] Schaate, A.; Roy, P.; Godt A.; Lippke, J.; Waltz, F.; Wiebcke, M.; Behrens, P. Modulated synthesis of Zr-based metal–organic frameworks: From Nano to single crystals. *Chem.—Eur. J.* **2011**, *17*, 6643–6651.

[40] Eddaoudi, M.; Kim, J.; Rosi, N.; Vodak, D.; Wachter, J.; O'Keeffe, M.; Yaghi, O. M. Systematic design of pore size and functionality in isoreticular MOFs and their application in methane storage. *Science* **2002**, *295*, 469–472.

[41] Carboni, M.; Lin, Z. K.; Abney, C. W.; Zhang, T.; Lin, W. B. A metal-organic framework containing unusual eight-connected Zr-oxo secondary building units and orthogonal carboxylic acids for ultrasensitive metal detection. *Chem.—Eur. J.* **2014**, *20*, 14965–14970.

[42] Li, Y. A.; Yang, S.; Li, Q. Y.; Ma, J. P., Zhang, S. J.; Dong, Y. B. UiO-68-ol NMOF-based fluorescent sensor for selective detection of HClO and its application in bioimaging. *Inorg. Chem.* **2017**, *56*, 13241–13248.

[43] Manna, K.; Zhang, T.; Carboni, M.; Abney, C. W.; Lin, W. B. Salicylaldimine-based metal–organic framework enabling highly active olefin hydrogenation with iron and cobalt catalysts. *J. Am. Chem. Soc.* **2014**, *136*, 13182–13185.

[44] Dolgopolova, E. A.; Ejegbavwo, O. A.; Martin, C. R.; Smith, M. D.; Setyawan, W.; Karakalos, S. G.; Henager, C. H.; Loye, H. C. Z.; Shustova, N. B. Multifaceted modularity: A key for stepwise building of hierarchical complexity in actinide metal-organic frameworks. *J. Am. Chem. Soc.* **2017**, *139*, 16852–16861.

[45] He, Y.; Hou, Y. L.; Wong, Y. L.; Xiao, R.; Li, M. Q.; Hao, Z.; Huang, J.; Wang, L.; Zeller, M.; He, J. Improving stability against desolvation and mercury removal performance of Zr(IV)-carboxylate frameworks by using bulky sulfur functions. *J. Mater. Chem. A* **2018**, *6*, 1648–1654.

[46] Li, B. J.; Gui, B.; Hu, G. P.; Yuan, D. Q.; Wang, C. Postsynthetic modification of an alkyne-tagged zirconium metal-organic framework via a "click" reaction. *Inorg. Chem.* **2015**, *54*, 5139–5141.

[47] Huang, H. B.; Sato, H.; Aida, T. Crystalline nanochannels with pendant azobenzene groups: Steric or polar effects on gas adsorption and diffusion? *J. Am. Chem. Soc.* **2017**, *139*, 8784–8787.

[48] Schukraft, G. E. M.; Ayala, S. Jr.; Dick, B. L.; Cohen, S. M. Isoreticular expansion of polyMOFs achieves high surface area materials. *Chem. Commun.* **2017**, *53*, 10684–10687.

[49] Jiang, H. L.; Feng, D. W.; Liu, T. F.; Li, J. R.; Zhou, H. C. Pore surface engineering with controlled loadings of functional groups via click chemistry in highly stable metal-organic frameworks. *J. Am. Chem. Soc.* **2012**, *134*, 14690–14693.

[50] Gui, B.; Meng, X. S.; Chen, Y.; Tian, J. W.; Liu, G. L.; Shen, C. C.; Zeller, M.; Yuan, D. Q.; Wang, C. Reversible tuning hydroquinone/ quinone reaction in metal-organic framework: Immobilized molecular switches in solid state. *Chem. Mater.* **2015**, *27*, 6426–6431.

[51] Luo, T. Y.; Liu, C.; Eliseeva, S. V.; Muldoon, P. F.; Petoud, S.; Rosi, N. L. Rare earth pcu metal-organic framework platform based on RE4(μ3-OH)4(COO)6 2+ clusters: Rational design, directed synthesis, and deliberate tuning of excitation wavelengths. *J. Am. Chem. Soc.* **2017**, *139*, 9333–9340.

[52] Wang, R. M.; Zhang, M. H.; Liu, X. B.; Zhang, L. L.; Kang, Z. X.; Wang, W.; Wang, X. Q.; Dai, F. N.; Sun, D. F. Tuning the dimensionality of interpenetration in a pair of framework-catenation isomers to achieve selective adsorption of CO2 and fluorescent sensing of metal ions. *Inorg. Chem.* **2015**, *54*, 6084–6086.

[53] Oisaki, K.; Li, Q. W.; Furukawa, H.; Czaja, A. U.; Yaghi, O. M. A metal–organic framework with covalently bound organometallic complexes. *J. Am. Chem. Soc.* **2010**, *132*, 9262–9264.

[54] Liu, L.; Wang, X. J.; Zhang, Q.; Li, Q. W.; Zhao, Y. L. Distinct interpenetrated metal–organic frameworks constructed from crown ether-based strut analogue. *CrystEngComm* **2013**, *13*, 841–844.

[55] Zhang, C. L.; Hao, H.; Shi, Z. Z.; Zheng, H. G. Four new metalorganic frameworks based on a rigid linear ligand: Synthesis, optical properties and structural investigation. *CrystEngComm* **2014**, *16*, 5662–5671.

[56] Sahu, J.; Ahmad, M.; Bharadwaj, P. K. Structural diversity and luminescence properties of coordination polymers built with a rigid linear dicarboxylate and Zn(II)/Pb(II) ion. *Cryst. Growth Des.* **2013**, *13*, 2618–2627.

[57] Prasad, T. K.; Suh, M. P. Metal–organic frameworks incorporating various alkoxy pendant groups: Hollow tubular morphologies, X-ray single-crystal structures, and selective carbon dioxide adsorption properties. *Chem.—Asian J.* **2015**, *10*, 2257–2263.

[58] Hauptvogel, I. M.; Biedermann, R.; Klein, N.; Senkovska, I.; Cadiau, A.; Wallacher, D.; Feyerherm, R.; Kaskel, S. Flexible and hydrophobic Zn-based metal-organic framework. *Inorg. Chem.* **2011**, *50*, 8367–8374.

[59] Sahu, J.; Aijaz, A.; Xu, Q.; Bharadwaj, P. K. A three-dimensional pillared-layer metal-organic framework: Synthesis, structure and gas adsorption studies. *Inorg. Chim. Acta* **2015**, *430*, 193–198.

[60] Singh, R.; Bharadwaj, P. K. Coordination polymers built with a linear bis-imidazole and different dicarboxylates: Unusual entanglement and emission properties. *Cryst. Growth Des.* **2013**, *13*, 3722−3733.

[61] Dutta, G.; Jana, A. K.; Singh, D. K.; Eswaramoorthy, M.; Natarajan, S. Encapsulation of silver nanoparticles in an amine-functionalized porphyrin metal–organic framework and its use as a heterogeneous catalyst for CO2 fixation under atmospheric pressure. *Chem.—Asian J.* **2018**, *13*, 2677–2684.

[62] Liu, X. Y.; Liu, B.; Li, G. H.; Liu, Y. L. Two anthracene-based metal-organic frameworks for highly effective photodegradation and luminescent detection in water. *J. Mater. Chem. A* **2018**, *6*, 17177–17185.

[63] Feng, D. W.; Wang, K. C.; Wei, Z. W., Chen, Y. P.; Simon, C. M.; Arvapally, R. K.; Martin, R. L.; Bosch, M.; Liu, T. F.; Fordham, S. et al. Kinetically tuned dimensional augmentation as a versatile synthetic route towards robust metal-organic frameworks. *Nat. Commun.* **2014**, *5*, 5723.

Broto et al., Figure 1

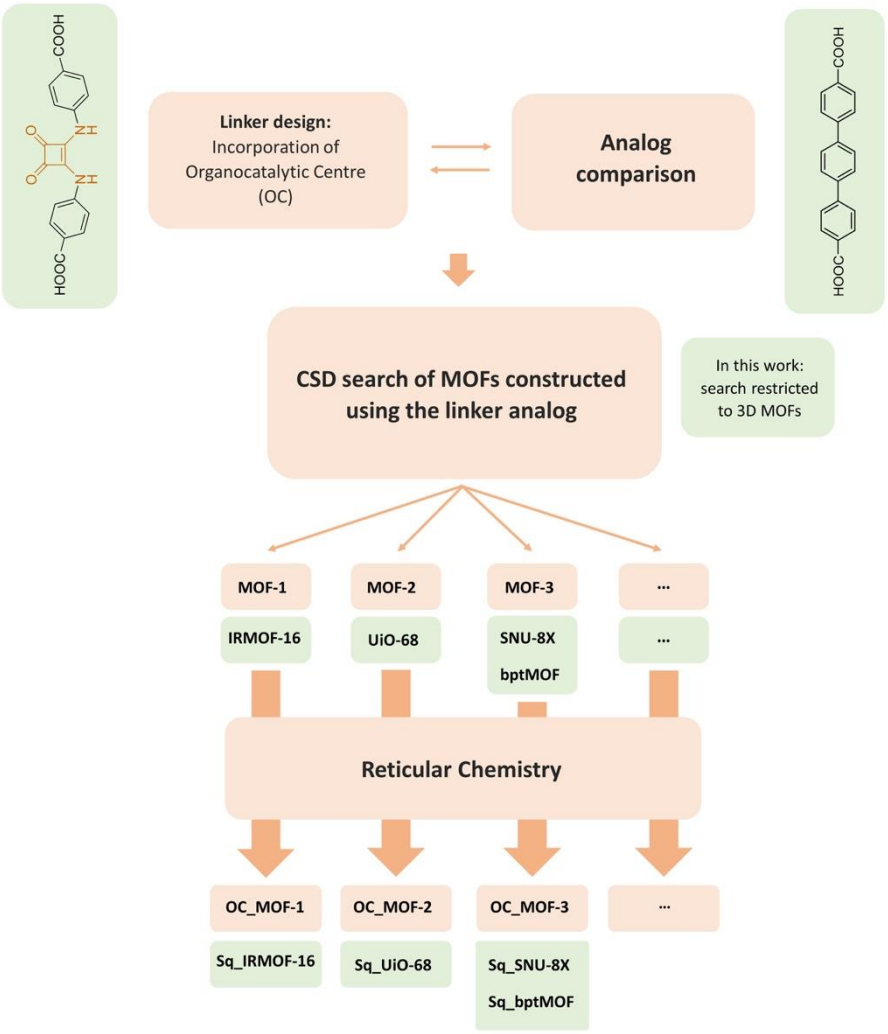

Figure 1. The reticular chemistry-based strategy for rational design of MOF-based catalysts containing organocatalytic centers. CSD: Cambridge Structural Database.

Broto et al., Figure 2

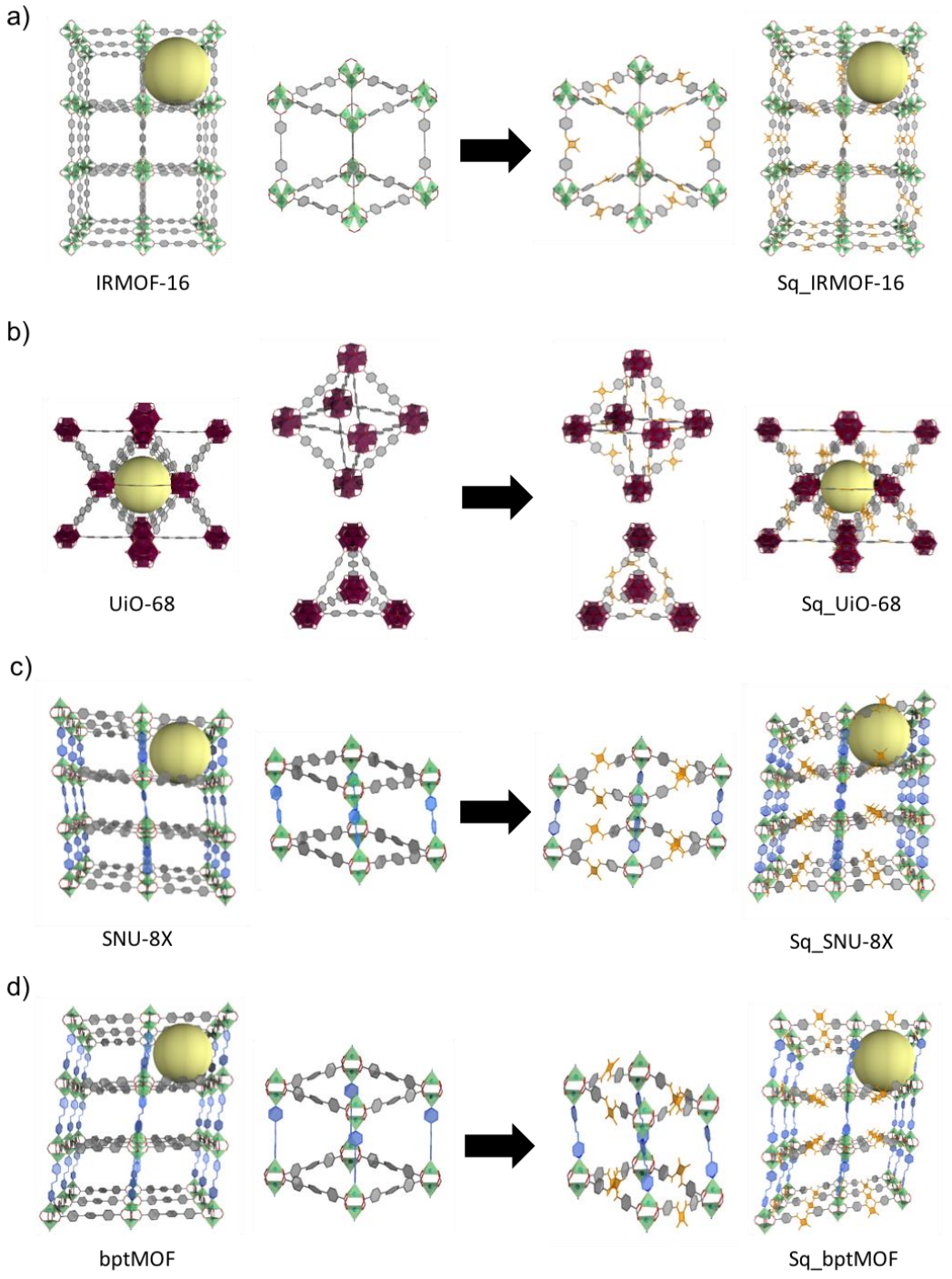

Figure 2. Representation of the crystal structures and cavities/pores of the MOFs and their corresponding isoreticular analogs (containing the squaramide rings): **IRMOF-16** and **Sq_IRMOF-16** (a); **UiO-68** and **Sq_UiO-68** (b); **SNU-8X** and **Sq_SNU-8X** (c); and **OZASUF** and **Sq-bptMOF** (d).

Broto et al., Figure 3

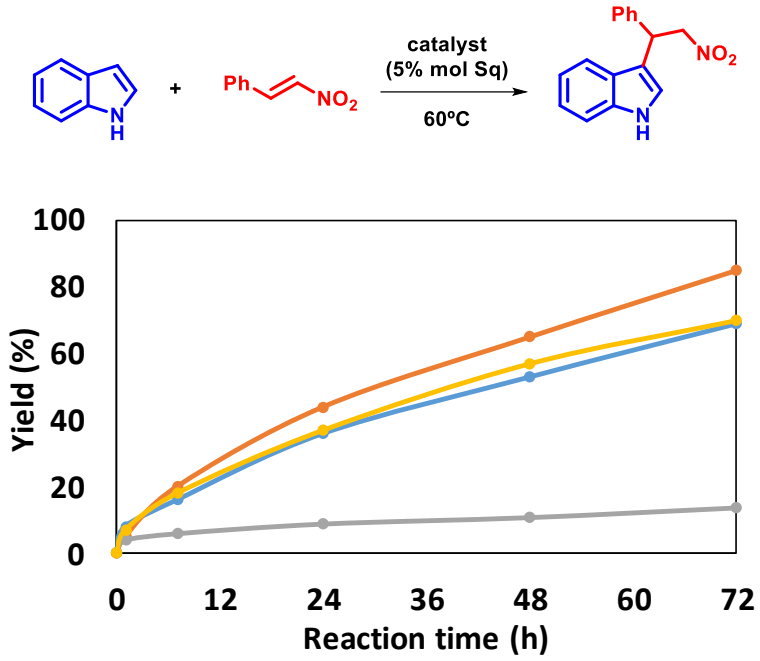

Figure 3. Kinetic plots for the Friedel-Crafts reaction of indole and β-nitrostyrene at 60 ºC, forming the alkylated product, in the presence of **Sq_IRMOF-16** (yellow), **Sq_SNU-8X** (orange), **Sq_UiO-68** (blue) or **Sq_bptMOF** (grey).

Broto et al., Figure 4

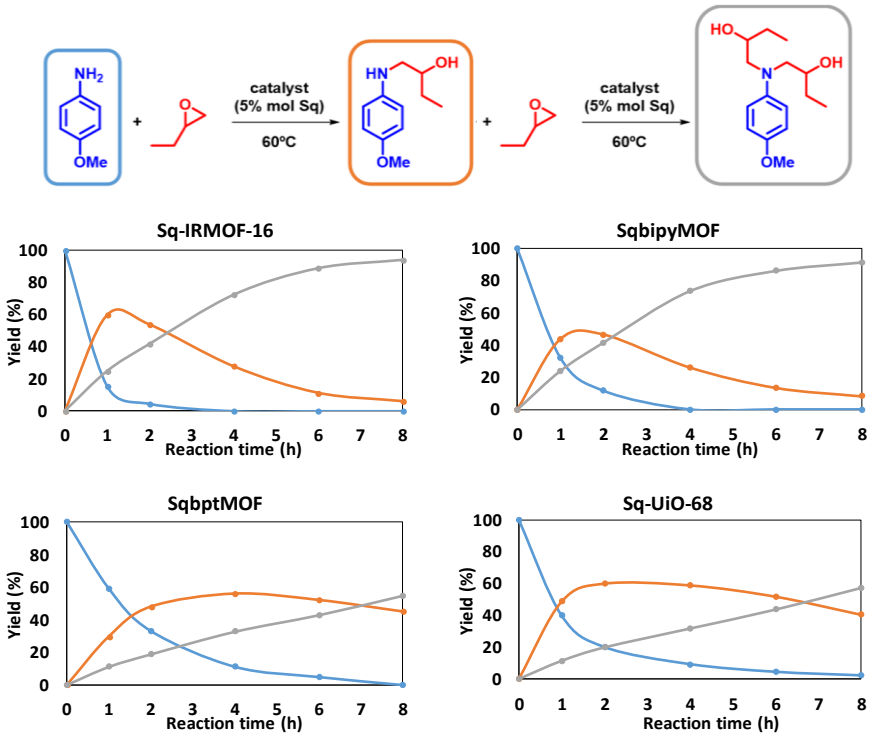

Figure 4. Kinetic plots for the epoxide ring-opening reaction of 4-methoxy aniline (blue) and ethyl epoxide at 60 °C to form the mono-adduct (orange) or bis-adduct (grey) product, in the presence of **Sq_IRMOF-16**, **Sq_SNU-8X**, **Sq_UiO-68** or **Sq_bptMOF**.